COUPLED EVALUATION OF BELOW- AND ABOVE-GROUND ENERGY AND WATER CYCLE VARIABLES FROM REANALYSIS PRODUCTS OVER FIVE FLUX TOWER SITES IN THE U.S.

by

William Lytle

A Thesis Submitted to the Faculty of the

DEPARTMENTS OF ATMOSPHERIC SCIENCES AND HYDROLOGY AND WATER RESOURCES

In Partial Fulfillment of the Requirements

For the Degree of

MASTER OF SCIENCE

WITH A MAJOR IN HYDROMETEOROLOGY

In the Graduate College

THE UNIVERSITY OF ARIZONA

2015

STATEMENT BY AUTHOR

The thesis titled Coupled Evaluation of Below- and Above-Ground Energy and Water Cycle Variables from Reanalysis Products Over Five Flux Tower Sites in the U.S. prepared by William E. Lytle has been submitted in partial fulfillment of requirements for a master's degree at the University of Arizona and is deposited in the University Library to be made available to borrowers under rules of the Library.

SIGNED: William Lytle

APPROVAL BY THESIS DIRECTOR

This thesis has been approved on the date shown below:

_____	August 26, 2015
Xubin Zeng	Date
Professor of Atmospheric Science	

Abstract

Reanalysis products are widely used to study the land-atmosphere exchanges of energy, water, and carbon fluxes, and have been evaluated using in situ data above or below ground. Here measurements for several years at five flux tower sites in the U.S. (with a total of 315,576 hours of data) are used for the coupled evaluation of both below- and above-ground processes from three global reanalysis products and six global land data assimilation products. All products show systematic errors in precipitation, snow depth, and the timing of the melting and onset of snow. Despite the biases in soil moisture, all products show significant correlations with observed daily soil moisture for the periods with unfrozen soil. While errors in 2 meter air temperature are highly correlated with errors in skin temperature for all sites, the correlations between skin and soil temperature errors are weaker, particularly over the sites with seasonal snow. While net shortwave and longwave radiation flux errors have opposite signs across all products, the net radiation and ground heat flux errors are usually smaller in magnitude than turbulent flux errors. On the other hand, the all-product averages usually agree well with the observations on the evaporative fraction, defined as the ratio of latent heat over the sum of latent and sensible heat fluxes. This study identifies the strengths and weaknesses of these widely-used products, and helps understand the connection of their errors in above- versus below-ground quantities.

1. Introduction

Due to a lack of globally consistent observational data, reanalysis products have become invaluable tools in earth sciences (Kalnay et al. 1996). Reanalysis products are generated by assimilating remotely sensed and in-situ data into global models to produce gridded data sets that provide a best possible representation of the state of the climate system (Balsamo et al. 2013; Reichle et al. 2011; Rienecker et al. 2011; Dee et al. 2011; Saha et al. 2010; Rodell et al. 2004). However, they are still subject to errors contained in the model physics. These products are also often used to drive land surface models (LSMs; Qian et al. 2006), which are in turn used for the production of gridded data sets used in climate studies (Bengtsson et al. 2004**)**, and to force hydrologic models (Lauri and Kummu 2014). The increased use of reanalysis products in the scientific community combined with their potential for inherent errors has dictated the need for a careful evaluation of their skill (Wang and Zeng 2012; Decker et al. 2011; Reichle et al. 2011; Mao et al. 2010).

For instance, Decker et al. (2011) used flux tower measurements to perform a comprehensive evaluation of the 6- hourly and monthly outputs of atmospheric variables used to force LSMs along with near surface turbulent energy and water fluxes. This was done for reanalysis products from the National Aeronautics and Space Administration (NASA) Global Modeling and Assimilation Office (GMAO), National Oceanic and Atmospheric Administration (NOAA) National Centers for Environmental Prediction (NCEP), and European Centre for Medium-Range Weather Forecasts (ECMWF). They found that overall the ECMWF- Interim Reanalysis (ERA-Interim) performed the best, with at least part of its accuracy owing to the assimilation of 2 m air temperature. However, they showed that the Climate Forecast System Reanalysis (CFSR) outperforms the ERA-Interim, the Modern-Era Retrospective Analysis for

Research Applications (MERRA), and the Global Land Data Assimilation (GLDAS) in its representation of 6-hourly latent heat flux; this is attributable to CFSR's use of precipitation in the land data assimilation. Additionally they showed that GLDAS performs the best for producing precipitation totals due to the use of observed precipitation data as a forcing field for LSMs.

Reichle et al. (2011) assessed the skill (defined as the correlation of the bias of product time series from the observed climatology) of MERRA-Land, MERRA, and ERA-Interim compared with in-situ observations. The assessment was conducted for root zone soil moisture, snow depth, snow water equivalent (SWE), and runoff. They showed that the skill of MERRA and MERRA-Land is typically higher than that of ERA-Interim with MERRA-Land typically performing slightly better than MERRA. These results are attributed to additional observational fields of surface forcing data included in MERRA-Land and the model physics improvement compared with MERRA. Wang and Zeng (2012) evaluated daily and monthly values of six reanalysis products over the Tibetan Plateau using 62 weather stations. They found that no one reanalysis product could be considered superior to any other for all variables or timescales and thus suggested that multiple products be used in weather and climate studies of the region.

Evaluation studies conducted so far either included a large collection of reanalyses and focused entirely on atmospheric outputs (Decker et al. 2012), or examine above- and below-ground fields with a small number of products only (Reichle et al. 2011). However, the question still remains: how do both (surface-atmosphere) coupled and offline land (non-coupled) products compare to one another and to observations in their outputs of above- and below-ground fields?

The above evaluation studies focused on the atmospheric variables predominately used in the forcing of LSMs; furthermore these studies focused on hourly or monthly timescales.

However the output fields from LSMs (e.g. soil moisture and temperature, snow depth and snow water equivalent) have a strong seasonal variability and are of particular importance in studying the phenomena associated with the hydrologic cycle. For instance, Betts et al. (2014) found that, over the Canadian Prairies, snow cover acts as a rapid catalyst for seasonal climatic transitions. They showed that near surface air temperature falls by 10 K within days of the surface experiencing snow cover in the autumn with a similar rise in temperature corresponding to the melting of snow in the spring. They also showed that, with a 10% drop in the number of days experiencing snow cover, the mean winter temperature there rose by 1.4 K.

Nigam and Ruiz-Barradas (2006) performed a seasonal evaluation of ECMWF's 40-year reanalysis (ERA-40) along with the NCEP reanalysis, the North American Regional Reanalysis (NARR) and several climate models using gridded and remotely sensed data. They found that the difference between summer and winter product errors of surface air temperature is 5-9 K larger than observations for climate models and upwards of 4 K larger for reanalysis, suggesting that the reanalyses and models are more sensitive to the seasonal change than nature.

The importance of the seasonal variations highlighted by Betts et al. (2014) combined with inherent errors of reanalysis products highlighted by Nigam and Ruiz-Barradas (2006) suggests that an evaluation of the seasonal behavior of the land surface components of reanalysis products and the recently developed off-line land based reanalyses is needed. More explicitly, the question becomes: are the known seasonally dependent errors of Nigam and Ruiz-Barradas (2006) present in below-surface fields as well and are these seasonal errors linked to the transition between snow-cover and snow-free periods?

This study performs just such an evaluation utilizing 6 reanalysis products: MERRA, MERRA-Land, ERA-Interim, ERA-Land, CFSR, and GLDAS. The evaluation is conducted

using flux towers along with stations from the Cooperative Observer Network (COOP) over the continental United States. The focus is on the seasonal (summer to winter and vice versa) transition of near surface variables: air and skin temperatures, precipitation, snow depth, snow water equivalent, surface energy and radiation fluxes, and below-surface variables of soil temperature and moisture.

2. Data Description and Methods

a. In-Situ Observation

In-situ measurements for this study were taken from five flux tower sites from the AmeriFlux network within the FLUXNET database (http://www.fluxnet.ornl.gov; Baldocchi et al. 2001). FLUXNET is a global network of flux tower sites that use eddy covariance techniques to make measurements of water, energy and CO_2 exchanges. This study analyzes the non gap-filled level two data of: 2-meter air temperature, skin temperature, soil temperature and moisture, and surface energy and radiation fluxes from the FLUXNET sites. Details of the sites used are provided in Table 1, while a map of all sites used can be seen in Figure S1. The sites were chosen so as to represent a variety of land cover types, while being located in an area of sufficiently homogenous land cover and terrain so as to be probably representative of an entire model grid box for a given reanalysis product. Sites were also chosen to have at least four years of continuous data between 2000 and 2007. All sites have either half hourly or hourly data output frequencies; these are averaged to create a six hourly time series so as to be directly comparable with all reanalysis fields.

These flux tower sites, however, do not provide the in-situ snow depth and precipitation measurements that are crucial for our analysis. These observations are therefore taken from the

National Weather Service (NWS) Cooperative Observer Program (COOP) (data accessed from http:://rda.ucar.edu.edu/datasets/ds510.0/). COOP data incorporates observations from NWS principal climatological stations, Federal Aviation Administration, National Park Service, Bureau of Land Management, and United States Geologic Survey. COOP data is available, dating back to 1854 and covering the United States, the Virgin Islands, Puerto Rico and assorted Pacific Islands. Observations of daily snow depth and precipitation are used for this study. The COOP archiving system considers snow depth less than 0.5 inches and precipitation less than 0.005 inches to be a trace amount and recorded as zero inches.

COOP stations employed here are within 60 km of a flux tower and are at an elevation within 105 m of the tower elevation. Stations are also chosen with similar topographic and land cover profiles as the flux tower. Data from these stations is then averaged together to create a single data set (Figure S1).

To help address the spatial representativeness issue of in-situ snow measurements, we also use the gridded snow depth product from the Canadian Meteorological Centre (CMC; Brown and Brasnett 2010). This data set is on a 24 km polar stereographic grid and covers the period from 1998 to 2013 for the Northern Hemisphere and contains daily fields of snow depth. The dataset is an interpolation of a combination of data from synoptic observations, meteorological aviation reports, and special aviation reports. Data are available at ftp://sidads.colorado.edu/pub/DATASETS/nsidc0447_CMC_snow_depth_v01/

b. Reanalysis Products

A short description of the surface-atmosphere coupled and land surface offline reanalysis products used in this study follows, highlighting the major differences between the products

primarily in the near surface and subsurface aspects of the products and their assimilation of near surface forcing fields (e.g. observed and satellite derived precipitation). More detailed descriptions are available from the relevant references.

To address the issue of a lack of assimilated land surface data, ECMWF and GMAO have developed offline (not coupled to the atmosphere) re-runs of their reanalysis products: ERA-Interim/Land (hereafter ERA-Land) (Balsamo et al. 2013) and MERRA-Land (Reichle et al. 2011) respectively. The re-runs utilize atmospheric output fields from the original reanalysis products along with observed precipitation data to force improved LSMs, in order to better capture surface and subsurface fields and the complete hydrologic cycle. For the same reason, GLDAS products are also used here.

MERRA (available at http://mirador.gsfc.nasa.gov/) is a NASA produced product covering the satellite era, from 1979 to present and is available in near real time. MERRA makes use of the Goddard Earth Observing System Data Assimilation System (GEOS-5) Atmospheric General Circulation Model (AGCM) (Rienecker et al. 2011) to produce hourly outputs at a native latitude-longitude resolution of ½º× ⅔º. MERRA assimilates instantaneous rain rate from the Special Sensor Microwave Imager (SSM/I) and the Topical Rainfall Measuring Mission (TRMM) (Rienecker et al. 2011). It also uses a catchment based land model (Koster et al. 2000).

MERRA-Land is forced entirely with output surface meteorological fields from MERRA with the exception that the MERRA-Land precipitation is corrected towards gauge measurements via the Global Precipitation Climatology Project (GPCP) version 2.1 (Reichle et al. 2011). Furthermore MERRA-Land benefits from a set of improved hydrological treatments, particularly related to rainfall interception that allows a greater amount of rainfall to reach the soil. Covering the same time period with the same spatial and temporal frequency as MERRA,

MERRA-Land introduces several additional hydrological and subsurface fields (e.g. soil temperature). MERRA-Land data can be found along with MERRA data at http://mirador.gsfc.nasa.gov/.

ERA-Interim (available http://apps.ecmwf.int/datasets/) is the fully coupled reanalysis product from ECMWF (Simmons et al. 2006). It covers the period from 1979 to present, with a spectral resolution of T255 (~79 km). ERA-Interim employs a four-dimensional variational data assimilation (4DVar), which is more advanced than the three-dimensional variational data assimilation (3DVar) employed by all other reanalysis products utilized in this study. Observed in-situ 2 m air temperature and humidity are also assimilated. ERA-Interim uses a 12 hour assimilation period. All variables analyzed here are taken at 6 hourly intervals. Because analysis fields for surface energy fluxes (latent and sensible heat, along with radiative fluxes at the surface) and precipitation are not available, they are taken from the 6 hour intervals of forecast fields initiated at 0000 UTC (Simmons et al. 2006).

In much the same style as MERRA-Land, ERA-Land is an offline reanalysis product with meteorological forcing provided by ERA-Interim and operating with the same temporal and spatial resolution as ERA-Interim (Balsamo et al. 2010). As with MERRA-Land, ERA-Land benefits from a bias correction of ERA-Interim precipitation, using GPCP v2.1. ERA-Land also uses a newer version of the LSM within ERA-Interim, with improved snow treatment (Dutra et al. 2010), a satellite based vegetation climatology (Boussetta et al. 2012), an improved bare soil evaporation scheme (Balsamo et al. 2011), and improved soil hydrology (Balsamo et al. 2009). As with ERA-Interim, fields are used at 6 hour intervals with sensible heat, latent heat, net radiation, and precipitation fields taken from the reanalysis forecast. ERA-Land can be accessed at http://apps.ecmwf.int/datasets/ along with the ERA-Interim data.

GLDAS (accessible at http://mirador.gsfc.nasa.gov/) is an offline land data assimilation product that uses a single set of atmospheric forcing fields to drive four different LSMs (Rodell et al. 2004). These forcing data come from a variety of sources; for a complete list see http://ldas.gsfc.nasa.gov/gldas/GLDASforcing.php. GLDAS uses these data to drive four different LSMs: Mosaic (Koster and Suarez 1996), the Community Land Model (CLM) (Dai et al. 2003), Noah (Ek et al. 2003), and the Variable Infiltration Capacity (VIC) model (Liang et al. 1996). GLDAS outputs three hourly data covering the satellite era, from 1979 to present. This is done at several different spatial resolutions; however, only 1º × 1º resolution for each LSM are analyzed in this study (Rodell et al. 2004).

The reanalysis product from NCEP (CFSR) also covers from 1979 to present (Saha et al. 2010). CFSR is an atmosphere-ocean coupled reanalysis at T382 (~38 km) horizontal resolution. CFSR uses gauge based gridded precipitation data to drive its Noah LSM. The data assimilation process operates on a 6-hourly cycle and the product outputs forecast data at each hour between the analysis periods (Saha et al. 2010). However, only the 6-hourly analysis outputs are considered for this study. CFSR data is available from several locations including http://rda.ucar.edu/datasets/ds093.0/

3. Results

Not every product produces all fields of interest for this study; Table S1 shows which variables are analyzed from which products. Our analysis will focus on the WI (forest) and MT (grassland) sites (Figs. 1 and 2) as representative case studies with other site results discussed in tables. Three separate groups of fields will be analyzed: water cycle including precipitation, snow depth and soil moisture; temperature including soil, skin, and 2 m air temperatures; and

surface energy fluxes, including sensible, latent, and ground heat fluxes, as well as upward and downward shortwave and longwave radiation fluxes.

a. Water Cycle

For all sites there are clear patterns in the temporal variation of water cycle variable errors. Products tend to misrepresent the peak depth of snow and the snow period as can be seen in Figures 1, 2, and S2 (top middle panel). The onset of the snow period is taken as the first day with a snow depth greater than 1.3 cm or SWE greater than 0.13 cm (chosen to correspond to the minimum recorded values at the COOP stations) that is followed by a period of more than three days with snow on the ground within the next fourteen days. This is done so as to exclude small early season isolated storms not corresponding to the onset of winter snow cover. The snow period is defined as having ended when the depth or SWE values drop below the above thresholds and stay there for a period of fourteen days.

Table 2 shows the discrepancies in the snow fields for the three (WI, MT, and IN) sites with snow. Because snow depth is only provided for the MERRA and ERA reanalysis, timing of snow fall and melt is taken from the SWE fields of other products. The MERRA and MERRA-Land products have the greatest errors in the timing of first snowfall and snow melt and consistently overestimate the snow period with delays on the order of months. The GLDAS products capture the timing of snow well, as they are all driven by the same observed precipitation data. It is still surprising, however, that the different criteria used to separate snow versus rain in the four land models (CLM, Mosaic, Noah, and VIC) in GLDAS lead to different snowfall onset dates by up to 29 days (over the MT site between CLM and VIC). The peak snow

depth error is within 6 cm at MT, but can be as large as 13 cm at IN (by MERRA-Land) and 18 cm in magnitude at WI (by ERA-Interim) (Table 2).

While the in situ observations are based on the average of several COOP sites (4 at WI, 4 at MT, and 3 at IN), they still don't represent the grid box average. We could use the differences between in situ data and CMC results to roughly estimate the uncertainty due to spatial representativeness issues. Then Table 2 shows that most products perform well in the first snowfall date (except MERRA and MERRA-Land, and ERA-Interim at IN). In contrast, all products perform poorly in capturing the snow end date over at least one site (except GLDAS-VIC). Overall, ERA-Land performs best in the maximum snow depth.

The precipitation differences between various products and the in situ data are presented in the top left panel of Figures 1, 2 and S2-S4. They are also summarized in Table 3. Some of these differences may be partially caused by the scale mismatch between point measurements and grid box averages. However, even the differences between different products are very large (e.g., 4.2 mm/day over the FL site between the different global precipitation products in GLDAS versus CFSR in summer). As was also shown by Decker et al (2011) the precipitation differences tend to be greater in magnitude for the June-August (JJA) period than for the December-February (DJF) period (Table 3), likely because of large convective storms in summer as can be seen in Figures 1, 2, and S2-S4.

In general, SWE is driven by snowfall and constrained by sublimation and snowmelt. SWE is linked to snow depth via the snow density. Therefore, large errors in precipitation in a product are likely to indicate large errors in snow depth. However several products actually show opposite signs in precipitation and snow depth errors. For example all products show a negative November precipitation bias in MT, but the multi-product mean shows a positive snow depth

bias in November (top panels of Figure 2). In contrast, these biases change signs in February/March.

Soil moisture errors tend to be smaller at WI and IN with greater average soil moisture (Figures 1 and S2) compared with those at MT and AZ (Figures 2 and S3). For sites in WI, MT, IN, and AZ (as soil moisture data is unavailable for FL), the average (across all products) correlation coefficient between observed daily soil moisture and product soil moisture for days with unfrozen soil is 0.39, 0.45, 0.65, and 0.66 respectively, all significant at the 99% level. The correlation is largest at the snow-free AZ site and is the smallest at the WI site receiving the most annual snow, partly contributed by snow errors in all products.

b. Temperature

The soil temperature fields of the various reanalysis products are produced for different depths below the surface. For each product the level that most closely corresponds to 5 cm is chosen and is given in Table S1. Soil levels for in-situ measurements are given in Table 1. Unless otherwise denoted the 5 cm or 4 cm levels are used for analysis.

The monthly mean diurnal cycle for soil temperature at WI is shown in Figure 3, and the results here are representative of those at the other sites. For January and February, all products show a colder soil temperature than in-situ observations. For June and July, some products show a greater diurnal variation and most have a warmer bias.

In general, soil temperature is a function of soil depth, and this factor should be considered when in-situ data is used to evaluate various products. To address this issue, observations at two depths are shown in Figure 3, and their differences are generally much smaller in magnitude than those between products and observations. This suggests that soil

temperature biases of various products are not caused by the soil depth differences between products and measurements in Figure 3.

The semi-arid AZ site has a higher soil temperature gradient with depth and a larger spread of results from the various products (Figure S3). The largest differences occur in the late afternoon and in midsummer (figure not shown). At these times the difference in observed soil temperature at the two depths of 4 cm and 8 cm represent at most 35% of the spread of the reanalysis products, and this ratio is much lower for nighttime temperatures. This gives confidence that the findings discussed here are not the result of discrepancies between reanalysis and observational soil depths, particularly for daily and monthly averaged quantities.

Soil temperature shows a shift in the sign of the error from negative in winter to positive in summer at the forested sites of WI (Figure 1), IN (Figure S2), and FL (Figure S4), and from positive in winter to negative in summer from the grassland site in MT (Figure 2). In contrast, the sign does not change at the shrubland site in AZ (Figure S3). This shift in sign of the error does not occur with the onset and departure of snow (Figure 1 and S2). Furthermore, this effect is seen not just in the daily mean, but also in the mean diurnal cycle (Figure 3). Consistent with the seasonal shift of errors over the three forested sites, reanalysis products show a mean soil temperature seasonal cycle amplitude (taken as the difference in the average temperature in JJA from DJF 7.2ºC, 6.2ºC, and 2.8ºC greater than observations for WI, IN, and FL respectively.

Over the forested WI site, the magnitude of the errors increases from skin temperature down to 5 cm soil temperature during the snow-covered period (middle panels of Figure 1), and the reanalysis products show an average of 2.8ºC greater seasonal amplitude than skin temperature observations (versus 7.2ºC for soil temperature difference). For the AZ site (without

snow), there is an average yearly negative bias in soil temperature of -4.2 ºC and -6ºC for skin temperature.

To understand the above results, we need to recognize that the 2 meter air temperature and skin temperature are linked through turbulent mixing, while the skin and soil temperatures are linked through the snow and soil heat transfer. Table 4 quantifies the correlations between the errors of these three temperatures. At the three sites (WI, IN, and MT) with seasonal snow, the correlation of the errors is highest between air and skin temperatures. The weaker correlation between skin and soil temperatures is partly caused by the snow biases, leading to the greater soil temperature bias in magnitude than the skin temperature bias at WI, as mentioned earlier. At AZ, the correlations of air temperature with both skin and soil temperatures are high (Table 4), and the heat transfer in the soil naturally leads to the lower soil temperature bias in magnitude than the skin temperature bias, as mentioned earlier.

Noah and CLM have similar correlations between air and skin temperature errors, because they are both driven by the same air temperature data in GLDAS. In contrast, they have larger differences in the correlations between air (or skin) and soil temperature errors, partly because soil temperature is strongly dependent on land models. Note that, because soil temperature is also dependent on soil moisture which is strongly affected by precipitation and snowmelt, the use of the same land model in GLDAS-Noah and CFSR does not lead to the same correlations between skin and soil temperatures (Table 4).

c. Energy Fluxes

Daily ground heat flux (GH) is typically well represented by all reanalysis products (e.g., Figures 1, 2, and S2-S4). The average magnitude of GH errors for the various products is

comparable and usually within 10 W/m^2, with CFSR typically having the poorest representation of GH (Table 5). In the two snow free sites, daily GH errors average -3.3 Wm^{-2} (at AZ) and 6.7 Wm^{-2} (at FL) only, with standard deviations of 3.5W/m^2 and 0.2 W/m^2 among different products, respectively. At the sites with seasonal snow coverage (WI, MT, and IN), the GH error is usually highest around snowmelt time (Figures 1, 2, and S2). For instance, the average GH error in the week proceeding and following snowmelt increases from the annual mean error by 10.6 Wm^{-2} for MERRA at the WI site and by 18.1 Wm^{-2} from GLDAS-Mosaic. This feature is more likely tied to errors in the products' peak snow depth, because the spike in GH errors initiates just before snow melt begins when the snow depth is the greatest and it is not strongest in MERRA and MERRA-Land even though they have the poorest representation of the snow melt time.

The errors in latent (LH) and sensible heat (SH) fluxes are generally greater than the GH errors in magnitude (Figs. 1, 2, S2-S4, and Table 5). In particular, the all-product averages overestimate LH over all sites except AZ (Figs. 1, 2, and S2-S4), consistent with the finding of Decker et al. (2011). For the sites with snow, these LH errors are generally greater during the snow-free period when LH itself is large due to the increase in net radiative fluxes (Figs. 1, 2, and S2). However there is a decrease in the positive bias of nearly all products timed with peak summer rainfall. Not surprisingly there is a significant spike in SH errors (Figure 4) during this time to account for the energy surplus no longer being attributed to LH.

Both LH and SH errors are related to the net radiative flux errors. To isolate the LH and SH errors that are less affected by the radiative flux errors, Figure 5 shows the evaporative fraction (EF), defined as LH/(SH + LH), for the observations and the products (averaged together for clarity) along with observed daily precipitation. Over the FL, AZ, and MT sites, the all-product averages agree very well with the observations, including the spike of EF during the

period of peak summer rains. At the IN and WI sites, while observations show a spike in EF in the early summer and then a nearly constant EF during the summer and early fall, the all-product averages show a nearly constant EF for the whole snow-free period. This indicates that, on average, the products at the WI and IN sites fail to capture the seasonal transition in the partitioning of surface available energy.

GH, SH, and LH are driven and balanced by the net radiative fluxes (defined as downward minus upward radiative fluxes). In general net shortwave radiation tends to be overestimated while net longwave radiation is underestimated (Table 5). The underestimate of net longwave radiation flux is likely linked to summer warm bias (e.g., Figs. 1, 2, S2, and S3). Figure 4 shows the average across all products of the SH, LH, net shortwave (SW) and net longwave (LW) radiation for WI in order to show the temporal evolution of the errors in these fields. The positive bias in net shortwave radiation along with the negative bias in net longwave radiation results in a surplus of net radiative flux at the surface. For the snow-covered period (from day 321 to day 105) in Figure 4, the average (across all products) net shortwave and longwave flux errors are 4.6 and -12.8 Wm^{-2}, leading to a net radiative flux error of -8.2 Wm^{-2}. The average errors in LH (10.8 Wm^{-2}) and SH (-12.8 Wm^{-2}) are comparable in magnitude but have opposite signs. For late spring and early summer when soil is relatively wet (day 106 to day 175) in Figure 4, the net radiative flux error of 22.2 Wm^{-2} is overly balanced by the LH error of 45.5 Wm^{-2} (with a smaller compensational SH error of -14.7 Wm^{-2}). For late summer and early fall when the soil is drier (day 176 to day 320), the average SH error (12.7 Wm^{-2}) becomes positive, but it is still smaller than the LH error (17.8 Wm^{-2}).

All products have a small residual in the energy balance (SW+LW+GH-SH-LH), usually within 2 Wm^{-2} in magnitude. In contrast, flux tower sites do not maintain closure in the energy

budget (Wilson et al. 2002), partly because the covariance methods used by the towers do not account for all methods by which energy is transported including subsidence and horizontal advection (Foken et al. 2011). For the four sites (WI, IN, MT, and AZ), the residuals are 21.8, 37.7, -12.2, and 9.2 Wm^{-2}, respectively.

In order to better quantify errors in the SH and LH fields, while considering the lack of closure of the energy budget at the flux tower sites, we have forced the monthly energy budget into closure in the flux tower data by multiplying the SH and LH terms by a constant scale factor, A, for each month such that: SW+LW+GH-A*(SH+LH) = 0. This method preserves the EF while providing a closed observational energy budget by which we can better evaluate SH and LH from reanalysis products. This adjustment would shift the SH errors from the above values to -16.5 Wm^{-2}, -35.6 Wm^{-2}, and 7.4 Wm^{-2} for the snow covered, moist soil, and dry soil portions of the year described earlier. For the same periods the LH errors become: 10.2 Wm^{-2}, 27.0 Wm^{-2}, and -6.3 Wm^{-2}, respectively. These LH and SH errors follow a similar temporal pattern before or after adjustment, only with the addition of a seasonal oscillation in the sign of the errors occurring as the soil begins to dry.

4. Conclusions

In this study, we have used the in-situ data for several years over five flux tower sites (with a total of 315,576 hours of data) to evaluate above- and below-ground quantities as well as interface quantities from three global reanalysis products (MERRA, ERA-Interim, CFSR) and six global land data assimilation products (MERRA-Land, ERA-Land, and GLDAS with CLM, Mosaic, Noah, and VIC). These five sites cover major land cover types over midlatitudes (three forest sites, one grassland site, and one shrubland site) with seasonal snow cover over three sites.

All of the reanalysis products analyzed in this study show systematic errors in their representations of soil moisture, snow depth and precipitation. Precipitation tends to be underestimated by the reanalyses, with a significant increase in this negative bias occurring with the summer rains. The exception to this pattern is that MERRA and MERRA-Land have slight positive biases during the summer rains, at the AZ, FL and MT sites. Consistent with the precipitation bias, snow depth is subject to large errors as well, and the error of -18 cm in maximum snow depth (ERA-Interim in WI) is the greatest in magnitude for any product at any site. While some products (e.g., ERA-Land) realistically simulate the onset and ending dates of the snow season, MERRA and MERRA-Land tend to greatly overestimate the length of time with snow on the ground. This is significant because the disappearance of snow on the ground acts as fast switch that significantly increases air temperature and relative humidity (Betts et al. 2014). Despite the biases in soil moisture, all products show significant correlations with observed daily soil moisture for the periods with unfrozen soil, with the coefficients lower at the sites with the greatest snowfall (WI and MT).

Temperature fields at the forested sites (WI, IN, and FL) show a consistent seasonal shift in the behavior of the errors. Soil temperature error in these products is characterized by an underestimation during the winter, and a shift to an overestimation in summer. This leads to greater seasonal amplitude of soil temperature in these products over the three forested sites. This seasonal pattern is lacking from the 2 meter air temperature field. While errors in 2 meter air temperature are highly correlated with errors in skin temperature for all sites, the correlations between skin and soil temperature errors are weaker, particularly over the sites with seasonal snow (WI, IN, and MT). For instance, the all product-averaged positive air temperature error is greater than that of soil temperature at WI in summer, because air temperature is the driver of,

and strongly correlated with, soil temperature. In contrast, the negative air temperature error is smaller in magnitude than that of soil temperature in winter, because soil is shielded by snow and model deficiencies in snow biases become more important (in generating soil temperature errors).

There is a nearly pervasive positive bias in net shortwave radiation that peaks with the melting of snow, and a negative bias in net longwave radiation. This suggests that all products have an overestimation of the available energy at the surface. This available energy is partitioned into ground (GH) and turbulent (SH and LH) heat fluxes, with the GH errors usually smaller in magnitude than SH and LH errors. The all-product averages usually overestimate LH and underestimate SH. However, these biases change with season (e.g., for the snow period, spring/early summer with relatively wet soil, and summer/early fall with relatively dry soil). Furthermore, these biases are affected by the use of the original LH and SH measurements versus the adjusted values (to force energy balance in flux tower measurements).

Recognizing the energy flux imbalance issue in tower measurements, a more robust quantity is the evaporative fraction (EF), defined as LH/(SH + LH). Indeed the all-product averages usually agree well with the observed EF. For the springtime over WI and IN, however, the all-product averages show a nearly constant EF, which is different from the observed increase of EF with time.

It needs to be emphasized that there is an inherent uncertainty in using the point measurements to evaluate gridded products. While this uncertainty cannot be fully quantified in this study, we have attempted to address this issue from different perspectives. In Section 3a, we used several COOP sites for the in-situ snow data; used the differences between in-situ data and CMC results to roughly estimate the uncertainty due to spatial representativeness issues; and

identified large precipitation differences between reanalysis products (independent of in-situ data). In Section 3b, we used soil temperature measurements at two depths (rather than at a single depth) to evaluate reanalysis products; and evaluated relationships (between quantities) that may be less sensitive to spatial scaling issues than the quantities themselves (e.g., the correlation between air, skin, and soil temperatures and the seasonal shift of temperature errors). In Section 3c, we evaluated both EF (which may be less sensitive to scaling issues) and the actual SH and LH values with and without adjustments to close the energy budget in flux tower measurements.

Acknowledgements

This work was supported by NASA (NNX14AM02G) and NSF (AGS-0944101). We thank the data centers for providing various data sets for this work. The flux tower data was obtained from the FLUXNET database while the COOP and CFSR data was from the NCAR Research Data Archive (RDA). The MERRA, MERRA-Land, and GLDAS data were from the Goddard Earth Sciences (GES) Data and Information Services Center (DISC). ERA-Interim and ERA-Land were obtained directly from ECMWF. CMC data was acquired from the National Snow and Ice Data Center (NSIDC).

References:

Baldocchi, D., and Coauthors, 2001: FLUXNET: A new tool to study the temporal and spatial variability of ecosystem-scale carbon dioxide, water vapor, and energy flux densities. Bull. Amer. Meteor. Soc., 82, 2415-2434.

Balsamo, G. and Coauthors, 2009: A revised hydrology for the ECMWF model: Verification from field site to terrestrial water storage and impact in the Integrated Forecast System J. Hydrometeor., 10 623-643.

Balsamo, G., F. Pappenberger, E. Dutra, P. Viterbo and B. van den Hurk, 2010: A revised land hydrology in the ECMWF model: A step towards daily water flux prediction in a fully-closed water cycle, Special issue on large scale hydrology of Hydrol. Process., doi:10.1002/hyp.7808.

Balsamo, G., S. Boussetta, E. Dutra, A. Beljaars, P. Viterbo, and B. Van den Hurk, 2011: Evolution of land surface processes in the IFS. ECMWF Newsletter 127, 17-22.

Balsamo, G. and Coauthors, 2013: ERA-Interim/Land: a global land water resources dataset. Hydrol. and Earth Syst. Sci., 14705-14745.

Bengtsson, L., H. Stefan, and H. I. Kevin, 2004: Can climate trends be calculated from reanalysis data? J. Geophys. Res., 109, 1984-2012.

Betts, A. K., R. Desjardins, D. Worth, S. Wang, and J. Li, 2014: Coupling of winter climate transitions to snow and clouds over the Prairies. J. Geophys. Res-Atmo., 119, 1118-1139.

Boussetta, S., G. Balsamo, A. Beljaars, T. Kral, and L. Jarlan, 2012: Impact of a satellite-derived Leaf Area Index monthly climatology in a global Numerical Weather Prediction model. Int. J. Remote Sens. 34, 3520-3542.

Brown, R. D., and B. Brasnett, 2010: Canadian Meteorological Centre (CMC) Daily Snow Depth Analysis Data. National Snow and Ice Data Center, Environment Canada. [Available online at http://nsidc.org/data/nsidc-0447.html.]

Dai, Y., and Coauthors, 2003: The common land model. Bull. Amer. Meteor. Soc., 84, 1013-1023.

Decker, M., and Coauthors, 2012: Evaluation of the reanalysis products from GSFC, NCEP, and ECMWF using flux tower observations. J. Climate, 25, 1916-1944.

Dee, D. P., and Coauthors, 2011: The ERA Interim reanalysis: Configuration and performance of the data assimilation system. Q.J.R. Meteorol. Soc.,, 137, 553-597.

Dutra, E., and Coauthors 2010: An improved snow scheme for the ECMWF land surface model: description and offline validation J. Hydrometeor. 11, 899-916.

Ek, M. B., and Coauthors 2003: Implementation of Noah land surface model advances in the National Centers for Environmental Prediction operational mesoscale Eta model. J. Geophys. Res-Atmo., 108.D22.

Foken, T., M. Aubinet, J. J. Finnigan, M. Y. Leclerc, M. Mauder, and K. T. Paw U, 2011: Results off a panel discussion about the energy balance closure correction for trace gases. Bull. Amer. Meteor. Soc., 92, ES13–ES18.

Kalnay, E., and Coauthors, 1996: The NCEP/NCAR 40-Year Re- analysis Project. Bull. Amer. Meteor. Soc., 77, 437–471.

Koster, R. D., and M. J. Suarez, 1996: Energy and water balance calculations in the Mosaic LSM. NASA Tech. Memo 59.

Koster, R. D., M. J. Suárez, A. Ducharne, M. Stieglitz, and P. Kumar, 2000: A catchment-based approach to modeling land surface processes in a general circulation model: 1. Model

structure. J. Geophys. Res-Atmo., 105, 24809-24822.

Lauri, H., T. A. Räsänen, and M. Kummu, 2014: Using reanalysis and remotely sensed temperature and precipitation data for hydrological modelling in monsoon climate: case Mekong River. *J. Hydrometeor.,* 15, 1532-1545.

Liang, X., D. P. Lettenmaier, and E. F. Wood, 1996: One-dimensional statistical dynamic representation of subgrid spatial variability of precipitation in the two-layer variable infiltration capacity model. J. Geophys. Res-Atmo., 101, 21403-21422.

National Climatic Data Center/NESDIS/NOAA/U.S. Department of Commerce, National Weather Service/NOAA/U.S. Department of Commerce, and Federal Aviation Agency/U.S. Department of Transportation (1981), NCDC TD3200 U.S. Cooperative Summary of Day, 1890(1948)-cont, http://rda.ucar.edu/datasets/ds510.0/, Research Data Archive at the National Center for Atmospheric Research, Computational and Information Systems Laboratory, Boulder, Colo. (Updated monthly.)

Nigam, S., and A. Ruiz-Barradas, 2006: Seasonal hydroclimate variability over North America in global and regional reanalyses and AMIP simulations: Varied representation. *J. Climate,* 19, 815-837.

Mao, J., and Coauthors, 2010: Assessment of reanalysis daily extreme temperatures with China's homogenized historical dataset during 1979-2001 using probability density functions. *J. Climate,* 23.24. 6605-6623.

Qian, T., A. Dai, K. E. Trenberth, and K. W. Oleson, 2006: Simulation of global land surface conditions from 1948 to 2004. Part I: Forcing data and evaluations. *J. Hydrometeor.,*7 953-975.

Reichle, R. H., and Coauthors, 2011: Assesment of Enhancment of MERRA Land Surface

Hydrology Estimates. *J. Climate,* 24, 6322-6338.

Rienecker, M. M., and Coauthors, 2011: MERRA: NASA's modern-era retrospective analysis for research and applications. *J. Climate,* 24, 3624-3648.

Rodell. M., and Coauthors, 2004: The Global Land Data Assimilation System. *Bull. Amer. Meteor. Soc*., 8085, 381-394.

Saha, S., and Coauthors, 2010: The NCEP Climate Forecast System Reanalysis. *Bulletin of the American Meteorological Society* 91, 1015-1057.

Simmons, A., S. Uppala, D. Dee, and S. Kobayashi, 2006: ERA-Interim: New ECMWF reanalysis products from 1989 onwards. *ECMWF newsletter* 110, 25-35.

Wang, A., and X. Zeng, 2012: Evaluation of Multireanalysis Products With In Situ Observations Over The Tibetan Plateau. *J. Geophys. Res-Atmo., 117*, D05102

Wilson, K. B., and Coauthors, 2002: Energy balance closure at FLUXNET sites. *Agric. For. Meteor.,* 113, 223–243.

Table Captions:

Table 1. Description of flux tower sites used in this study. Only one principal investigator (PI) is listed (even though some sites have multiple Co-PIs).

Table 2. Errors in snow representation. Positive values in timing errors indicate either early snow fall or late snow melt such that positive values indicate more time with snow on the ground in a product than observations. Max snow depth error is taken as the average error for the 30 day period with the greatest snow depth in the observations. Results from products with the relevant variable are shown.

Table 3. Mean seasonal precipitation errors in mm/day for each product at each site. Note that GLDAS (Mosaic, CLM, Noah, and VIC) products use the same precipitation.

Table 4. Correlation coefficients of errors in different temperature fields for each product at each site. Blank spaces are left where a product does not have both fields, or where in-situ data is not available. Only values with * are not significant at the 99% level.

Table 5. Mean errors (between daily products and in situ data) (Wm-2) in surface net shortwave and longwave radiation (FL is excluded due to a lack of reliable data.), sensible heat, latent heat, and ground heat fields for each product at each site. Downward radiative and ground heat fluxes are defined to be positive, while upward latent and sensible heat fluxes are defined to be positive.

Figure Captions:

Figure 1. Errors between reanalysis and in situ flux tower and COOP observations for the WI site. For the upper row of water cycle variables, both the observed values (magenta histogram for precipitation and black line for daily snow depth and soil moisture) and the differences (red lines for the multi-product mean difference and blue lines for the maximum/minimum errors of the products) are shown, while only the differences are shown for the temperatures (middle row) and energy fluxes (bottom row). In the upper left panel the mean monthly precipitation errors from each product are shown along with the maximum/minimum monthly errors for the multi-year period. Vertical black lines show the date of snow melt, and first snow fall from left to right.

Figure 2. Same as Figure 1 but for the MT site.

Figure 3. Monthly mean diurnal cycle for soil temperature at the WI site. OBS and OBS2 refer to the measurements at 5cm and 10cm depths respectively.

Figure 4. Mean product errors for net shortwave and longwave radiation, sensible heat, and latent heat fluxes at WI. Downward radiative fluxes are defined to be positive, while upward latent and sensible heat fluxes are defined to be positive.

Figure 5. Black line shows daily EF from observations while red line is mean daily EF across all products during the snow-free period. Magenta histogram shows observed precipitation.

Table 1. Description of flux tower sites used in this study. Only one principal investigator (PI) is listed (even though some sites have multiple Co-PIs).

Name	State	Lat (ºN), Lon (ºW)	Period	Soil Levels (cm)	Land Cover	PI	Institution
Donaldson	FL	29.75, 82.16	2000-2007	5	Evergreen broad leaf	T. Martin	University of Florida
Santa Rita Mesquite	AZ	31.82, 110.87	2004-2007	4, 8	Open shrubland	R. Scott	USDA
Fort Peck	MT	48.31, 105.10	2000-2007	5, 10	Grassland	T. Meyers	NOAA
MorganMonroe State Forest	IN	39.32, 86.41	2000-2007	5	Deciduious broadleaf forest	K. Novick	Indiana Univ.
Willow Creek	WI	45.81, 90.80	2000-2007	5, 10	Deciduious broadleaf forest	P. Bolstad	University of Minnesota

Table 2. Errors in snow representation. Positive values in timing errors indicate either early snow fall or late snow melt such that positive values indicate more time with snow on the ground in a product than observations. Max snow depth error is taken as the average error for the 30 day period with the greatest snow depth in the observations. Results from products with the relevant variable are shown.

Variable	Product	IN	WI	MT
First snow fall date difference (days)	MERA	50	45	17
	MERLND	51	45	17
	CLM	-4	11	-37
	MOS	-4	11	-9
	Noah	-3	11	-9
	VIC	-4	11	-8
	ERAI	16	0	-11
	ERALND	4	1	-9
	CFSR	-1	-6	-9
	CMC	3	11	-8
Difference in the end of snow melt (days)	MERA	51	44	64
	MERLND	50	43	72
	CLM	10	-10	-38
	MOS	-53	-24	-6
	Noah	7	-21	-10
	VIC	10	5	-2
	ERAI	16	-12	4
	ERALND	4	-2	13
	CFSR	7	-2	19
	CMC	3	6	-8
Maximum snow depth difference (cm)	MERA	6	-10	-2
	MERLND	13	-7	6
	ERAI	1	-18	-5
	ERALND	1	-11	-4
	CMC	0.3	-7	-4

Table 3. Mean seasonal precipitation errors in mm/day for each product at each site. Note that GLDAS (Mosaic, CLM, Noah, and VIC) products use the same precipitation.

State	Period	MeraL	Merra	GLDAS	CFSR	ERAI	ERAL
WI	DJF	-0.1	0.1	-1.0	1.1	-0.5	0.0
	JJA	-1.4	-1.9	-3.2	-2.2	-2.8	-1.5
IN	DJF	-0.1	-0.2	-2.1	0.4	-1.4	-0.6
	JJA	-0.3	-1.4	-3.0	-1.8	-2.6	-1.2
MT	DJF	0.1	0.3	-0.2	0.7	0.1	0.1
	JJA	0.3	0.1	-1.1	-0.2	-0.9	0.0
AZ	DJF	-0.3	-0.2	-0.8	0.0	-0.4	-0.3
	JJS	0.1	0.2	-1.2	1.2	-0.6	0.0
FL	DJF	0.9	0.0	-0.8	0.9	-0.6	0.7
	JJA	1.7	2.0	-1.7	2.5	-0.9	1.4

Table 4. Correlation coefficients of errors in different temperature fields for each product at each site. Blank spaces are left where a product does not have both fields, or where in-situ data is not available. Only values with * are not significant at the 99% level.

Site	Product	Air/Skin	Air/Soil	Skin/Soil
WI	MERRA-LND	0.74	0.37	0.44
	CLM	0.77	0.45	0.44
	MOS	0.77		
	Noah	0.77	0.53	0.58
	ERA-I	0.72	0.37	0.46
	ERA-LND	0.57	0.26	0.48
	CFSR	0.74	0.23	0.31
IN	MERRA-LND		0.24	
	CLM		0.14	
	MOS			
	Noah		0.18	
	ERA-I		0.24	
	ERA-LND		0.25	
	CFSR		0.16	
MT	MERRA-LND	0.69	0.28	0.52
	CLM	0.80	0.33	0.32
	MOS	0.63		
	Noah	0.81	0.41	0.55
	ERA-I	0.70	0.43	0.47
	ERA-LND	0.60	0.45	0.70
	CFSR	0.77	0.44	0.63
AZ	MERRA-LND	0.78	0.58	0.93
	CLM	0.78	0.23	0.64
	MOS	0.63		
	Noah	0.85	0.74	0.94
	ERA-I	0.65	0.51	0.86
	ERA-LND	0.37	0.33	0.95
	CFSR	0.88	0.72	0.90
FL	MERRA-LND		0.29	
	CLM		-0.02*	
	MOS			
	Noah		-0.03*	
	ERA-I		-0.07	
	ERA-LND			
	CFSR		0.31	

Table 5. Mean errors (between daily products and in situ data) (Wm^{-2}) in surface net shortwave and longwave radiation (FL is excluded due to a lack of reliable data.), sensible heat, latent heat, and ground heat fields for each product at each site. Downward radiative and ground heat fluxes are defined to be positive, while upward latent and sensible heat fluxes are defined to be positive.

Site	Product	SW error	LW error	SH error	LH error	GH error
WI	MERRA-LND	18.6	-13.6	-3.8	23.0	-8.1
	MERRA	18.6	-13.6	-3.6	19.9	-8.1
	CLM	17.4	-14.5	5.2	10.7	-7.3
	MOS	18.9	-8.1	0.2	23.3	-7.7
	Noah	12.1	-16.2	-12.1	21.5	-8.1
	ERA-I	22.5	-16.0	-5.7	22.4	
	ERA-LND	26.3	-13.3	4.2	17.3	
	CFSR	2.0	-4.5	-8.1	20.7	-11.3
IN	MERRA-LND	3.1	-10.8	-4.7	37.2	0.3
	MERRA	3.1	-10.8	-1.7	30.9	0.2
	CLM	-0.7	-9.0	16.8	10.8	0.8
	MOS	1.9	-0.9	5.4	32.8	0.4
	Noah	-4.1	-10.6	-2.5	25.7	0.0
	ERA-I	-5.8	-9.7	-1.7	24.9	
	ERA-LND	6.2	-8.3	-3.4	32.9	
	CFSR	-12.4	-5.8	-4.8	26.8	-2.8
MT	MERRA-LND	26.0	-0.7	15.0	-1.1	-1.0
	MERRA	26.0	-0.7	9.5	1.4	-1.0
	CLM	13.8	-5.5	-0.2	-5.6	-0.1
	MOS	6.4	9.8	4.4	-2.3	-0.7
	Noah	17.2	-2.3	0.9	-0.6	0.2
	ERA-I	10.3	5.6	-6.8	3.3	
	ERA-LND	9.5	10.3	-1.4	5.2	
	CFSR	10.7	6.0	3.2	2.2	-5.0
AZ	MERRA-LND	6.5	-7.0	9.1	0.7	-2.0
	MERRA	6.5	-7.0	8.8	-1.9	-2.1
	CLM	-18.4	-1.2	-0.5	-12.1	-1.8
	MOS	-18.4	10.7	11.2	-11.7	-2.0
	Noah	-15.2	0.4	4.1	-11.3	-1.7
	ERA-I	9.7	-3.6	-4.4	13.0	
	ERA-LND	1.5	-7.5	-3.4	-0.4	
	CFSR	3.0	-4.5	21.2	-5.9	-10.6
FL	MERRA-LND			0.6	18.3	7.7
	MERRA			-2.5	19.0	7.7
	CLM			8.0	7.2	7.7
	MOS			1.1	25.0	7.7
	Noah			-5.5	14.4	7.3
	ERA-I			-5.5	17.1	
	ERA-LND			-6.8	28.1	
	CFSR			1.0	16.7	2.2

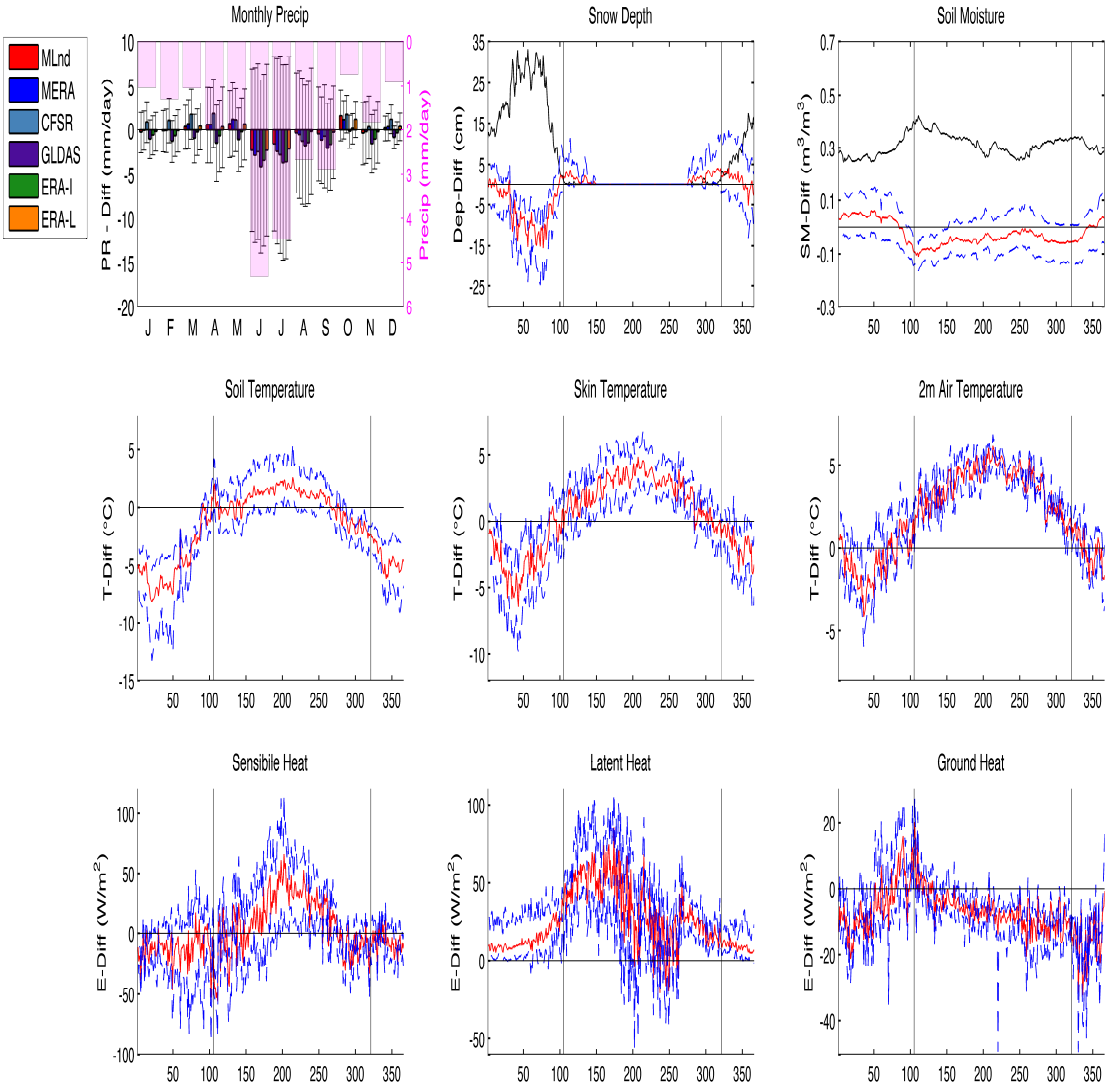

Figure 1. Errors between reanalysis and in situ flux tower and COOP observations for the WI site. For the upper row of water cycle variables, both the observed values (magenta histogram for precipitation and black line for daily snow depth and soil moisture) and the differences (red lines for the multi-product mean difference and blue lines for the maximum/minimum errors of the products) are shown, while only the differences are shown for the temperatures (middle row) and energy fluxes (bottom row). In the upper left panel the mean monthly precipitation errors from each product are shown along with the maximum/minimum monthly errors for the multi-year period. Vertical black lines show the date of snow melt, and first snow fall from left to right.

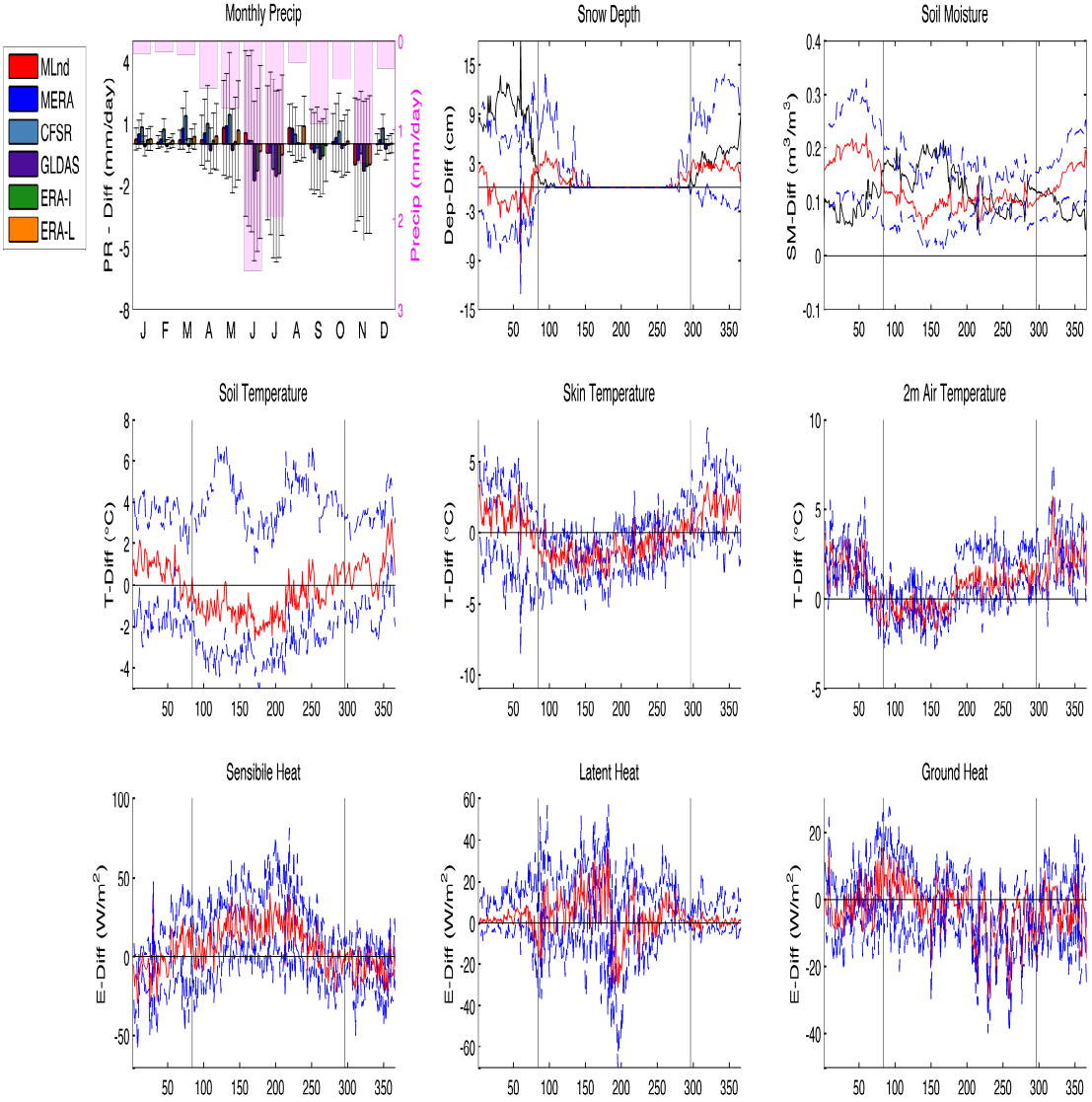

Figure 2. Same as Figure 1 but for the MT site.

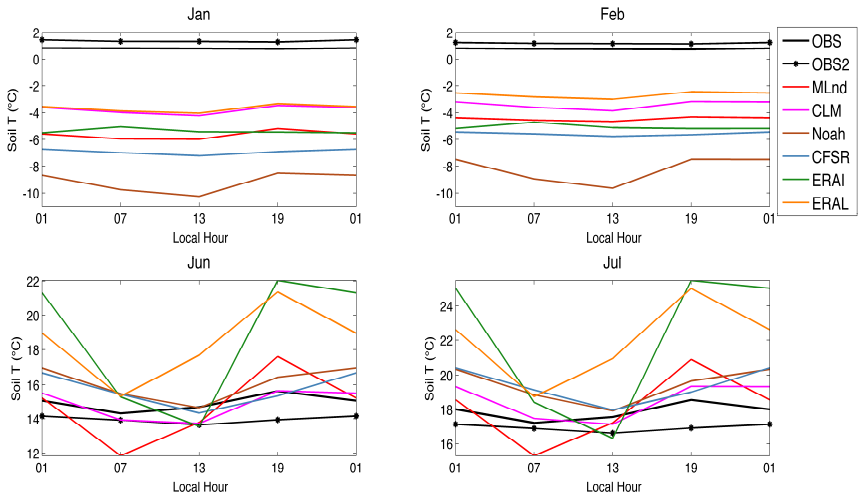

Figure 3. Monthly mean diurnal cycle for soil temperature at the WI site. OBS and OBS2 refer to the measurements at 5cm and 10cm depths respectively.

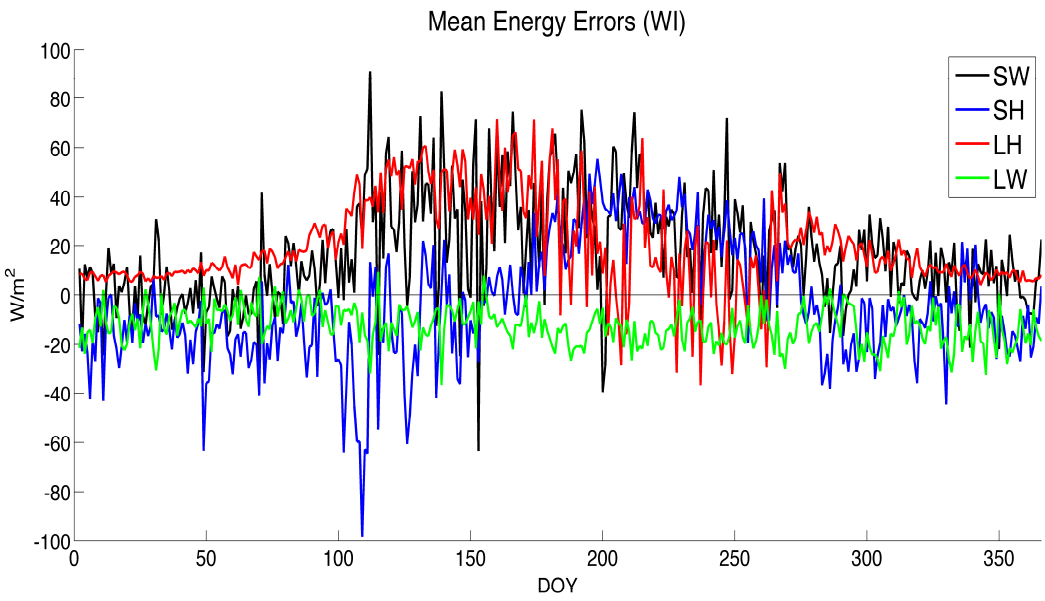

Figure 4. Mean product errors for net shortwave and longwave radiation, sensible heat, and latent heat fluxes at WI. Downward radiative fluxes are defined to be positive, while upward latent and sensible heat fluxes are defined to be positive.

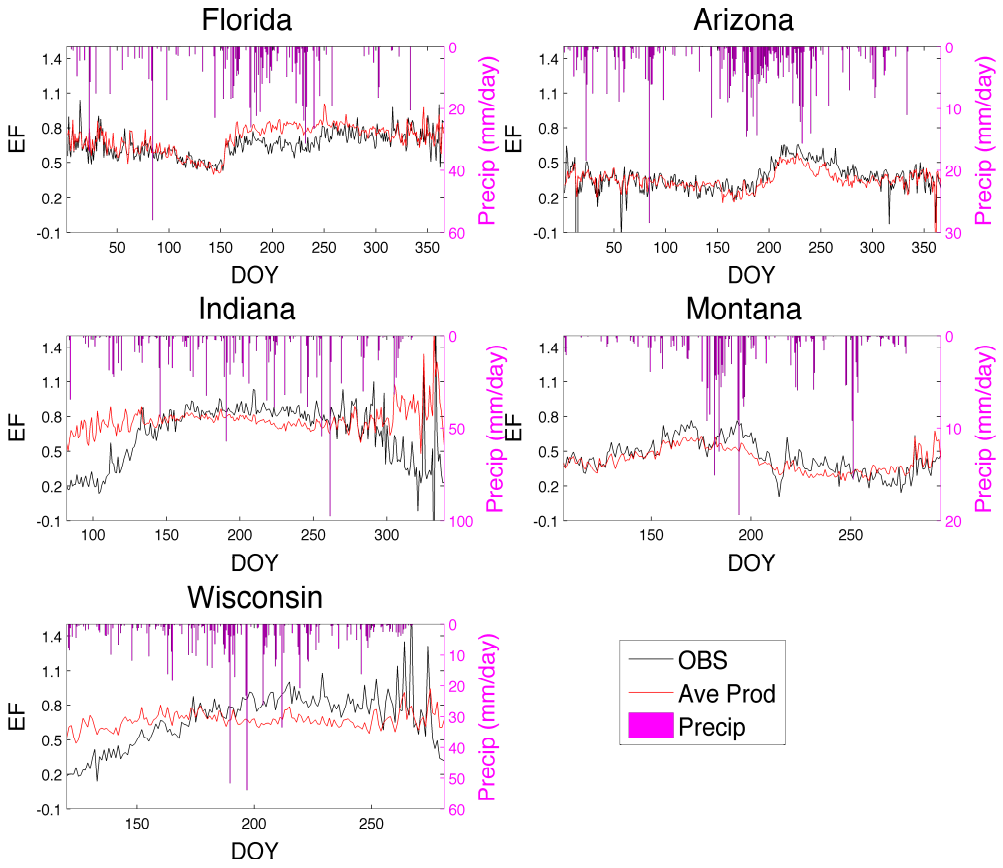

Figure 5. Black line shows daily EF from observations while red line is mean daily EF across all products during the snow-free period. Magenta histogram shows observed precipitation.